Directional Neighborhood Topologies Based Multi-Scale Quinary Pattern for Texture Classification

**ELMOKHTAR RACHDI[1], (Member, IEEE), YOUSSEF EL MERABET [1],
ZAHID AKHTAR [2], (Senior Member, IEEE), AND ROCHDI MESSOUSSI[1]**

[1]Laboratoire Systèmes Electroniques, Traitement de l'information, Mécanique et Energétique, Département de Physique, Faculté des Sciences, Université Ibn Tofail, Kénitra 14000, Morocco
[2]Department of Network and Computer Security, State University of New York Polytechnic Institute, Utica, NY 13502, USA

Corresponding author: Youssef El Merabet (youssef.elmerabet@uit.ac.ma)

ABSTRACT This paper ideates a new computationally simple and effective local image feature descriptor, referred to as Directional Neighborhood Topologies based Multi-scale Quinary Pattern (DNT-MQP) for texture description and classification. The essence of DNT-MQP is to encode the structure of local neighborhood by analyzing the differential excitation and directional information using various directional neighborhood topologies and new pattern encoding scheme. We first designed four different versions of single scale DNT-QP features based on four directional neighborhood topologies based sampling sets which are then combined together to build the effective multiscale DNT-MQP model. Unlike some existing parametric methods that employ static thresholds to perform thresholding, the construction process of DNT-MQP includes an automatic mechanism for dynamic thresholds estimation. Thanks to a richer local description ensured by exploiting complementary information resulting from single scale DNT-QP operators' combination, DNT-MQP descriptor has high capability to elicit stable and discriminative feature representation than other local feature descriptors. In addition, DNT-QP has the advantages of computational simplicity in feature extraction and low-dimensionality in feature representation. The effectiveness of DNT-QP is evaluated on sixteen challenging texture datasets and it is found that it maintains a high level of performance stability where the achieved performances are competitive or better than several recent most promising state-of-the-art texture descriptors as well as deep learning-based feature extraction approaches. Impressively, DNT-MQP showed good tolerance to rotation as well as illumination, scale and viewpoint changes against certain descriptors which are originally conceived to deal with these challenges. Furthermore, statistical hypothesis testing through Wilcoxon signed rank test is applied to prove the statistical significance of the accuracy improvement obtained in all the datasets.

INDEX TERMS Texture classification, texture recognition, texture descriptors, LBP, directional neighborhood topologies, local features.

I. INTRODUCTION

The surface of objects and materials such as crops in a field, natural scenes, human faces, palmprint, human skin and many others have their own distinctive texture. The texture analysis, which permits to provide constructive information about the structural and spatial arrangement of surfaces, has been extensively studied in the past few years and received considerable attention in many various research subjects such as pattern recognition, computer vision and image

The associate editor coordinating the review of this manuscript and approving it for publication was Wenming Cao.

processing. Texture classification is suitable for many potential applications for instance face classification and recognition, background subtraction, iris recognition, palmprint recognition [1], pedestrian detection, hyperspectral image classification [2], biomedical image analysis and image retrieval.

In the literature, there are many approaches available for texture analysis with excellent surveys given in [3]–[5]. One can cite human perception-based features [17], random features [15], filter-based techniques like Gaussian Markov random fields [13], Gabor [6] and wavelet [14], co-occurrence matrix-based approaches [7], ranklet

transform based approaches [16], fractal analysis based approaches [20], Texton dictionary-based [18], etc. The method proposed in [9] uses Fourier descriptors to extract texture feature in spectrum domain. Even though these above approaches, which take advantage of the merits of spectral and statistical features, ensure improving the ability of texture representation and modeling, their demerits lie in the fact that they increase the computation cost in extracting features. Therefore, local feature extraction methods have been proposed and have additionally and impressively been employed in texture analysis field. The main advantages of the local hand-crafted descriptors are the simplicity in design and not dependent upon a large volume of training data [39].

Among the local feature extraction approaches, local binary pattern (LBP) developed by Ojala *et al.* [8], have brightened up as one of the most eminent texture descriptor and has gained more attention over the past decades. LBP as an effective texture descriptor is, in fact, highly appreciated by researchers due to its distinctive advantages including its simplicity, its well invariability to monotonic gray level changes and its suitability for real time applications due to its low computing cost. The LBP method, even if originally designed for texture modeling and classification, it showed considerable performance in a wide range of applications like medical and biomedical images analysis, motion detection, image retrieval, face and facial description and recognition, background subtraction, etc. Despite these merits, the basic LBP descriptor has some limitations [49]: (1) the output is very sensitive even if to small change in the input; (2) it is not invariant to image rotation; (3) based on the employed thresholding scheme, it is highly susceptible to noise interference; etc. In order to deal with these limitations and thus enhance the classification performance of LBP, a great number of improved LBP algorithms have been proposed in recent years [21]–[23], [56], [69]. The authors in [5] provided an exhaustive investigation and comprehensive experiments assessing the performance of a great number of old and recent state-of-the-art texture descriptors in face recognition problem. The authors in [54] proposed one dimensional local binary patterns (1DLBP) for stone porosity computing using a new neighborhood topology and structure. Shiv *et al.* [53] designed local wavelet pattern (LWP) descriptor for medical image retrieval. LWP performs local wavelet decomposition over local neighborhood of pixels to encode the relation among the neighboring pixel. The LWP pattern for the central pixel is computed by comparing its local wavelet decomposed value with those of the neighboring pixels. Chakraborty *et al.* [47] introduced the local quadruple pattern (LQPAT) descriptor for using in facial image retrieval and recognition. LQPAT computes two micro patterns from the local relationships by encoding relations amongst the neighbors in quadruple space. In another study in [51] presented the center symmetric quadruple pattern (CSQP) descriptor for facial image retrieval and recognition. As for LQPAT, CSQP encodes the facial asymmetry in quadruple space. CSQP computes an eight-bit pattern from 16 pixels

in the local neighborhood. Issam *et al.* [57] proposed local directional ternary pattern (LDTP) for texture classification. LDTP, which exploits both LDP's and LTP's concepts, encodes both contrast information and directional pattern features in a compact way based on local derivative variations. Kas *et al.* [56] proposed mixed neighborhood topology cross decoded patterns (MNTCDP) for face recognition. MNTCDP adopts 5×5 block which allows combining radii (2) and angles (4) compared to 3×3 block supporting only angle variation.

The best position of hand-crafted descriptors has been dominated by LBP-like methods for more than a decade. The need to design an effective local texture descriptor with high discrimination capability is no longer to be demonstrated. Indeed, the development of methods based on local texture descriptors in pattern recognition continue to be designed still today, e.g., median local ternary patterns (MLTP) [50], averaged local binary patterns (ALBP) [58], repulsive-and-attractive local binary gradient contours (RALBGC) [52], local concave-and-convex micro-structure (LCCMSP) [49], attractive-and-repulsive center-symmetric local binary patterns (ARCS-LBP) [63], multi-direction local binary pattern (MDLBP) [37], improved local ternary patterns (ILTP) [55], quaternionic local angular binary pattern (QLABP) [61], selectively dominant local binary patterns (SDLBP) [62], chess pattern (Chess-pat) [59], multi level directional cross binary patterns (MLD-CBP) [60], synchronized rotation local ternary pattern (SRLTP) [38], oriented star sampling structure based multi-scale ternary pattern (O3S-MTP) [40], pattern of local gravitational force (PLGF) [39] and so on.

Even though LBP and its modifications and extensions achieve satisfactory performance, still an alternative technique to enhance the discriminative power in an image for effective texture modeling and representation is essential. In this paper, aiming at the further enhancement of texture classification performance and keeping the simplicity and effectiveness of the traditional LBP and addressing its feebleness, we design a conceptually simple and yet robust model of LBP, named directional neighborhood topologies based multi-scale quinary pattern (DNT-MQP). The designed texture operator has basically the following merits: As it will be shown further, DNT-MQP has low computational complexity and by offering highly-desirable features improves both the discriminative capability of LBP-like methods and their invariance to monotonic illumination changes as well as their robustness to small variations, due to image noise. The main contributions of this paper include the following:

- An automatic mechanism for dynamic thresholds estimation for quinary pattern creation process is proposed.
- A family of single scale descriptors named directional neighborhood topologies based single-scale quinary pattern (DNT-QP) is developed based on several directional neighborhood topologies (DNT) which are more effective for image texture understanding and analysis than large number of existing methods.

- We further extend the obtained single scale DNT-QP descriptors to incorporate multiscale by concatenating them into a single vector feature to build the effective directional neighborhood topologies based multi-scale quinary pattern (DNT-MQP) descriptor which should be more robust and stable.
- For performance evaluation, we restrict ourselves to texture classification as basic application of LBP. Extensive experiments on sixteen challenging publicly available texture database is performed.
- We provide a fair and systematic comparison and found that the designed texture operator shows superior performance to 34 recent powerful state-of-the-art texture descriptors.

The rest of the paper is organized as follows. Section II briefly introduces some typical existing texture descriptors. Section III presents the designed DNT-MQP descriptor. Comprehensive experimental results and comparative evaluation are given in Section IV. Section V concludes the study and presents some solid future research directions.

II. REVIEW OF THE EXISTING REPRESENTATIVE TEXTURE METHODS

In this part of study, we briefly introduce some of representative texture methods reported in the literature, our paper's core idea, contributions and organization. Given that the designed local texture descriptor is based on local kernel functions, it is appropriate to define the spatial arrangement of the local structure used in this paper. In this work, the choice was focused on the use of the 3×3 sized block given its easiness-of-implementation consideration and which is by far the most required neighborhood especially in real-time applications. The mathematical presentation of the set of gray-scale values of a 3×3 grayscale image patch $\mathbf{I}_{m,n}^{3 \times 3}$ around the central pixel $\mathbf{a}_c$ of coordinates (m,n) is given in Eq. 1.

$$\mathbf{I}_{m,n}^{3 \times 3} = \begin{bmatrix} \mathbf{a}_3 & \mathbf{a}_2 & \mathbf{a}_1 \\ \mathbf{a}_4 & \mathbf{a}_c & \mathbf{a}_0 \\ \mathbf{a}_5 & \mathbf{a}_6 & \mathbf{a}_7 \end{bmatrix} \quad (1)$$

$\mathbf{a}_p$ is the gray levels of the peripheral pixels (p $\in$ {0, 1,..., P-1}). P=8 is the number of local neighbors.

A. TRADITIONAL LOCAL BINARY PATTERNS

LBP method [8] characterizes the local spatial structure and the local contrast of each 3×3 local region in the image by thresholding the intensity of surrounding pixels $\mathbf{a}_p$; $p \in$ {0, 1, . . . , 7} with the intensity of the central pixel $\mathbf{a}_c$. The value of $\mathbf{a}_p$ is turned into binary value 1; otherwise, it is turned into 0. A code of 8 bits is obtained which is transformed into decimal number to get the LBP code. Formally, for a 3×3 local region, the definition of the kernel function of LBP operator is shown in the equation below:

$$f_{\text{LBP}}(\mathbf{I}_{m,n}^{3 \times 3}) = \sum_{p=0}^{\mathbf{P}-1} \vartheta(\mathbf{a}_p - \mathbf{a}_c) \times 2^p \quad (2)$$

where $\vartheta(\cdot)$ is the Heaviside step function (cf. Eq. (3)).

$$\vartheta(\mathbf{x}) = \begin{cases} 1, & \text{if } \mathbf{x} >= 0 \\ 0, & \text{otherwise} \end{cases} \quad (3)$$

Figure 1 shows the standard steps illustrating the process of the LBP feature extraction as well as the quantification of the difference between two texture images using LBP like features.
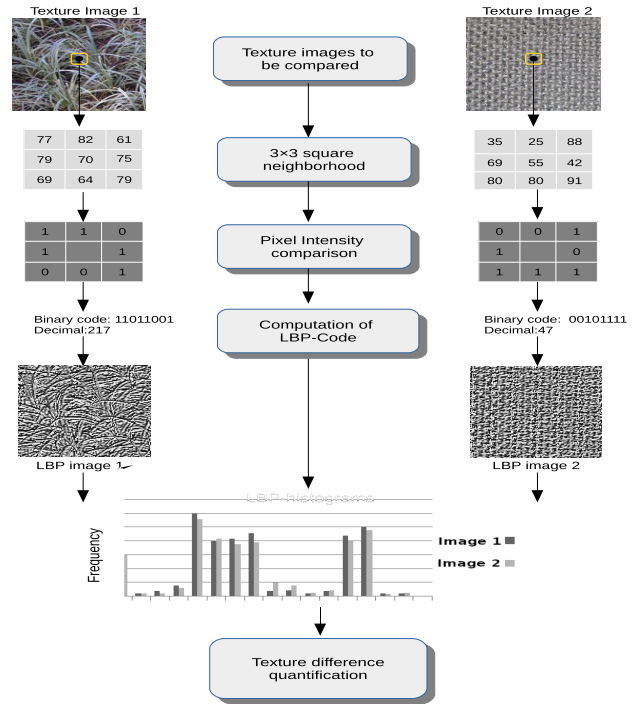

FIGURE 1. The standard steps for quantification of the difference between two texture images using LBP like features.

B. LOCAL QUINARY PATTERNS (LQP)

In local quinary patterns (LQP) [17], the difference of the gray level value between the central pixel $\mathbf{a}_c$ and its neighboring pixels $\mathbf{a}_p$ is encoded according to five levels (i.e., 2, −1, 0, 1 and 2) calculated using two thresholds τ_1 and τ_2. The LQP is thus closely relevant to the LTP [24], the only difference being that the number of coding levels is five in the LQP while in the LTP it is three. The quinary model is divided into four binary models according to the following rule:

$$\varphi_{LQP}(\mathbf{a}_p, \mathbf{a}_c, \tau_1, \tau_2) = \begin{cases} +2 & \mathbf{a}_p \geqslant \mathbf{a}_c + \tau_2, \\ +1 & \mathbf{a}_c + \tau_1 \leqslant \mathbf{a}_p < \mathbf{a}_c + \tau_2, \\ 0 & \mathbf{a}_c - \tau_1 \leqslant \mathbf{a}_p < \mathbf{a}_c + \tau_1, \\ -1 & \mathbf{a}_c - \tau_2 \leqslant \mathbf{a}_p < \mathbf{a}_c - \tau_1, \\ -2 & \text{Otherwise}, \end{cases}$$

$$(4)$$

where τ_1 and τ_2 are two user-specified parameters.

The LQP operator, by using the LTP's concept, splits each quinary pattern into four parts: LQP_{-2}, LQP_{-1}, LQP_{+1} and

LQP_{+2} which can be computed as follows(cf. Eqs. 12, 13, 14 and 15):

$$LQP_{-2}(\mathbf{I}_{m,n}^{3\times3}) = \sum_{p=0}^{7} \vartheta(\mathbf{a}_c - \mathbf{a}_p - \tau_2) \times 2^p \quad (5)$$

$$LQP_{-1}(\mathbf{I}_{m,n}^{3\times3}) = \sum_{p=0}^{7} \Big(\vartheta(\mathbf{a}_p - \mathbf{a}_c + \tau_2) \times \vartheta(\mathbf{a}_c - \mathbf{a}_p - \tau_1) \Big) \times 2^p \quad (6)$$

$$LQP_{+1}(\mathbf{I}_{m,n}^{3\times3}) = \sum_{p=0}^{7} \Big(\vartheta(\mathbf{a}_p - \mathbf{a}_c - \tau_1) \times \vartheta(\mathbf{a}_c - \mathbf{a}_p + \tau_2) \Big) \times 2^p \quad (7)$$

$$LQP_{+2}(\mathbf{I}_{m,n}^{3\times3}) = \sum_{p=0}^{7} \vartheta(\mathbf{a}_p - \mathbf{a}_c - \tau_2) \times 2^p \quad (8)$$

The four descriptor histograms generated by the four LQP_{-2}, LQP_{-1}, LQP_{+1} and LQP_{+2} operators are finally concatenated to form the final $\mathbf{h}_{LQP}$ future vector as illustrated in Eq. 9. LQP generates 4×2^8 possible different patterns.

$$\mathbf{h}_{LQP} = \big\langle \mathbf{h}_{LQP_{-2}}, \mathbf{h}_{LQP_{-1}}, \mathbf{h}_{LQP_{+1}}, \mathbf{h}_{LQP_{+2}} \big\rangle \quad (9)$$

C. IMPROVED LOCAL QUINARY PATTERNS (ILQP)

Armi *et al.* [35] proposed the improved local quinary patterns (ILQP) to overcome some disadvantages of LQP and thus improve its performance. The definition of the local quinary pattern in ILQP is the same as in the LQP operator. By contrast, the thresholds τ_1 and τ_2 are dynamically defined. τ_1 and τ_2 are computed as:

$$\tau_1 = median(|lmad - median(lmad)|); \quad (10)$$

where $lmad = \{LocalMAD_k | k = 1, 2, \ldots, M \times N\}$, $LocalMAD = median(|G - median(G)|)$ and $G = \{\mathbf{a}_p | p = 0; 1; \ldots; P - 1\}$

$$\tau_2 = \frac{1}{M \times N} \sum_{i=1}^{N} \sum_{j=1}^{M} LSV_{i,j}; \quad (11)$$

where M and N are the size of input image and $LSV_{i,j}$ is the local significant value of the neighborhood with center pixel c with coordination (i,j), given by $LSV_c = \frac{1}{P} \sum_{p=0}^{P-1}(|\mathbf{a}_c - \mathbf{a}_p|)$. The quinary pattern can be divided into the four local binary patterns as follows:

$$ILQP_{-2}(\mathbf{I}_{m,n}^{3\times3}) = \sum_{p=0}^{7} \vartheta(\mathbf{a}_c - \mathbf{a}_p - \tau_2) \times 2^p \quad (12)$$

$$ILQP_{-1,-2}(\mathbf{I}_{m,n}^{3\times3}) = \sum_{p=0}^{7} \Big[\Big(\vartheta(\mathbf{a}_p - \mathbf{a}_c + \tau_2) \times \vartheta(\mathbf{a}_c - \mathbf{a}_p - \tau_1) \Big) \\ | \vartheta(\mathbf{a}_c - \mathbf{a}_p - \tau_2) \Big] \times 2^p \quad (13)$$

$$ILQP_{+1,+2}(\mathbf{I}_{m,n}^{3\times3}) = \sum_{p=0}^{7} \Big[\Big(\vartheta(\mathbf{a}_c - \mathbf{a}_p + \tau_2) \times \vartheta(\mathbf{a}_p - \mathbf{a}_c - \tau_1) \Big)$$

$$| \vartheta(\mathbf{a}_p - \mathbf{a}_c - \tau_2) \Big] \times 2^p \quad (14)$$

$$ILQP_{+2}(\mathbf{I}_{m,n}^{3\times3}) = \sum_{p=0}^{7} \vartheta(\mathbf{a}_p - \mathbf{a}_c - \tau_2) \times 2^p \quad (15)$$

Note that the vertical bar | and × symbol stand for 'OR' and logical 'AND' operations, respectively.

III. PROPOSED METHOD

A. DIRECTIONAL NEIGHBORHOOD TOPOLOGIES BASED MULTI-SCALE QUINARY PATTEN

Considering the fact that a texture image is defined as the local spatial variations in pixel orientation and intensities, we design directional neighborhood topologies based multi-scale quinary patten (DNT-MQP) to describe the spatial variations in pixel intensities and orientation in a local neighborhood in the image. The essence of DNT-MQP is to perform local sampling and pattern encoding in the most informative directions contained within texture images. The construction process of the proposed DNT-MQP descriptor involves the following stages:

- STAGE #1 (Neighborhood topology): DNT-MQP descriptor considers a unit distance radius since closest neighboring pixels maintains more discriminating information for local texture descriptors keeping thus low computational complexity. Thus, the whole 3×3 grayscale image patch is adopted to design the DNT-MQP method which intends to explore the mutual information with respect to the adjacent neighbors. Consider the center pixel $\mathbf{a}_c$ and its 8 neighborhood pixels $\{\mathbf{a}_0, \mathbf{a}_1, \ldots \mathbf{a}_7\}$. On the basis of the above consideration, directional neighborhood topologies adopted by DNT-MQP and which are expected to better describe salient local texture structure are conducted as shown in Figure 2. The neighbors of a reference pixel $\mathbf{a_k}$ are categorized according to their angular position relative to that pixel. On the one side, from the first row of Figure 2, it can be inferred that the central pixel $\mathbf{a}_c$ is sampled each time with two pixels in each of four directions $\frac{(k\pi)}{4}$; $k \in \{0,1,2,3\}$. We consider four sets $S_{k;k\in\{0,1,2,3\}}$ of directional center-symmetric neighboring pixels with respect to directions $\frac{(k\pi)}{4}$ including the central pixel $\mathbf{a}_c$. Mathematical definition of $S_\mathbf{k}$ is given by Eq. 16.

$$Direction \frac{(\mathbf{k}\pi)}{4} : S_\mathbf{k} = \{\mathbf{a_k}, \mathbf{a}_c, \mathbf{a_{k+4}}\}; \quad (16)$$

On the other side, from the second row of Figure 2, it can be inferred that each peripheral pixel is sampled with two of its sequential peripheral neighboring pixels in each direction. We consider four new sets $\widetilde{S}_{\mathbf{k};\mathbf{k}\in\{0,1,2,3\}}$ of directional sequential peripheral neighbors with respect to directions $\frac{(2\mathbf{k}+1)\pi}{4}$. Mathematical definition of $\widetilde{S}_\mathbf{k}$ is given by Eq. 17.

$$Direction \frac{(2\mathbf{k}+1)\pi}{4} : \widetilde{S}_\mathbf{k} = \{\mathbf{a_{2k}}, \mathbf{a_{2k+1}}, \mathbf{a_{2k+2}}\} \quad (17)$$
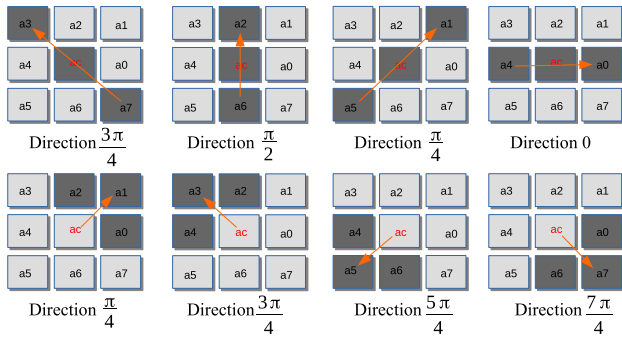
FIGURE 2. The adjacent neighbor relation for each of the 8 neighbors. (Top) the four sets of directional center-symmetric neighboring pixels and (Down) the four sets of directional peripheral neighboring pixels.

It appears from the literature that the average gray level as well as the median of the grey-scale values are widely accepted statistical parameters for texture analysis. In view of this and aiming at enhancing the thresholding range tolerance and thus finding a code which is insensitive to noise and more robust to illumination changes, several mean and median values (denoted as $\mathbf{a}_\mu$, $\mathbf{a}_{\widetilde{\mu}}$, $\mathbf{a}_{S_k}$, $\mathbf{a}_{\widetilde{S}_k}$, $\mathbf{a}_\varrho$ and $\mathbf{a}_{\widetilde{\varrho}}$) are incorporated as virtual pixels in the modeling of the proposed texture model. $\mathbf{a}_\mu$, $\mathbf{a}_{\widetilde{\mu}}$ are respectively the average local and global gray levels of the whole 3×3 square neighborhood and the whole image $I_{M \times N}$, $\mathbf{a}_{S_k}$ and $\mathbf{a}_{\widetilde{S}_k}$ are the average directional gray levels according to both sets S_k and $\widetilde{S}_k$ and $\mathbf{a}_\varrho$ and $\mathbf{a}_{\widetilde{\varrho}}$ are the median of the grey-scale values of the 3×3 square region and the whole image $I_{M \times N}$, respectively (cf. Eqs. 18, 19, 20 and 21).

$$\mathbf{a}_\mu = \frac{1}{9}\left(a_c + \sum_{p=0}^{P-1} \mathbf{a}_p\right) \qquad (18)$$

$$\mathbf{a}_{\widetilde{\mu}} = \frac{1}{M \times N} \sum_{i=0}^{M-1} \sum_{j=0}^{N-1} \mathbf{a}_{(i,j)} \qquad (19)$$

$$Direction\frac{(\mathbf{k}\pi)}{4} : \mathbf{a}_{S_k} = \frac{(\mathbf{a_k} + a_c + \mathbf{a_{k+4}})}{3} \qquad (20)$$

$$Direction\frac{(2\mathbf{k}+1)\pi}{4} : \mathbf{a}_{\widetilde{S}_k} = \frac{(\mathbf{a}_{2\mathbf{k}} + 2\mathbf{a}_{2\mathbf{k}+1} + \mathbf{a}_{2\mathbf{k}+2})}{4} \qquad (21)$$

The pixel samples of both S_k and $\widetilde{S}_k$ sets as well as the considered virtual pixels are then arranged into two directional neighborhood topologies based Sampling Sets, denoted as $\mathbb{SS}_1$ and $\mathbb{SS}_2$ (cf. Eqs. 22 and 23). The sampling set $\mathbb{SS}_1$ is constructed by considering the four couples of directional center-symmetric pixels $\{(\mathbf{a_k}, \mathbf{a_{k+4}}); \mathbf{k} \in \{0, 1, 2, 3\}\}$, the two couples of the average directional gray levels $\{(\mathbf{a}_{S_{2k}}, \mathbf{a}_{S_{2k+1}}); \mathbf{k} \in \{0, 1\}\}$ and the couple formed by the average local and global gray levels ($\mathbf{a}_\mu$ and $\mathbf{a}_{\widetilde{\mu}}$). In contrast, the sampling set $\mathbb{SS}_2$ is constructed by considering the four couples

of pixels $\{(\mathbf{a}_{2\mathbf{k}+1}, \mathbf{a}_{\widetilde{S}_\mathbf{k}}); \mathbf{k} \in \{0, 1, 2, 3\}\}$, the couple formed by the average local and global gray levels ($\mathbf{a}_\mu$, $\mathbf{a}_{\widetilde{\mu}}$) and the couple formed by the median of local and global the grey-scale values ($\mathbf{a}_\varrho$, $\mathbf{a}_{\widetilde{\varrho}}$). Mathematical definitions of both sampling sets $\mathbb{SS}_1$ and $\mathbb{SS}_2$ are given by Eqs. 22 and 23.

$$\mathbb{SS}_1 = \{(\mathbf{a}_\mu, \mathbf{a}_{\widetilde{\mu}}), (\mathbf{a}_{S_0}, \mathbf{a}_{S_1}), (\mathbf{a}_{S_2}, \mathbf{a}_{S_3}), \{(\mathbf{a_k}, \mathbf{a_{k+4}})\}\} \qquad (22)$$

$$\mathbb{SS}_2 = \{(\mathbf{a}_\varrho, \mathbf{a}_{\widetilde{\varrho}}), (\mathbf{a}_\mu, \mathbf{a}_{\widetilde{\mu}}), \{(\mathbf{a}_{2\mathbf{k}+1}, \mathbf{a}_{\widetilde{S}_\mathbf{k}})\}\} \qquad (23)$$

where $\mathbf{k} \in \{0, 1, 2, 3\}$.

- STAGE #2 (Pattern encoding): The local texture relationship between each couple of pixels within both sampling sets $\mathbb{SS}_1$ and $\mathbb{SS}_2$ and the central pixel, is encoded using a threshold values based LQP like coding scheme. The employed indicator function $\delta_0(\cdot, \cdot)$ that converts the couple relationship in quinary form is defined as follows (cf. Eq. 24):

$$\delta_0(\mathbf{a_x}, \mathbf{a_y}) = \begin{cases} 2, & \text{if } (\mathbf{a_x}, \mathbf{a_y}) \in \mathbb{SR}_{\tau_2}^U \\ 1, & \text{if } (\mathbf{a_x}, \mathbf{a_y}) \in \mathbb{SR}_{\tau_1}^U \\ -1, & \text{if } (\mathbf{a_x}, \mathbf{a_y}) \in \mathbb{SR}_{\tau_1}^L \\ -2, & \text{if } (\mathbf{a_x}, \mathbf{a_y}) \in \mathbb{SR}_{\tau_2}^L \\ 0, & \text{otherwise} \end{cases} \qquad (24)$$

where τ_1 and τ_2 ($\tau_2 > \tau_1$) are two positive user-specified parameters (i.e., thresholds) which are introduced to alleviate the effects of external factors such as noise which destabilizes the patterns. $\mathbb{SR}_{\tau_1}^U$, $\mathbb{SR}_{\tau_2}^U$, $\mathbb{SR}_{\tau_1}^L$ and $\mathbb{SR}_{\tau_2}^L$ are four Sets of pixels Relationship expressed in the following ways:

$$\mathbb{SR}_{\tau_1}^U = \{(\mathbf{a_x}, \mathbf{a_y}) \in \mathbb{SS}_1 | (\mathbf{a_x} \geqslant a_c + \tau_1) \& (\mathbf{a_y} \geqslant a_c - \tau_1)\} \qquad (25)$$

$$\mathbb{SR}_{\tau_1}^L = \{(\mathbf{a_x}, \mathbf{a_y}) \in \mathbb{SS}_1 | (\mathbf{a_x} \leqslant a_c - \tau_1) \& (\mathbf{a_y} \leqslant a_c + \tau_1)\} \qquad (26)$$

$$\mathbb{SR}_{\tau_2}^U = \{(\mathbf{a_x}, \mathbf{a_y}) \in \mathbb{SS}_2 | (\mathbf{a_x} \geqslant a_c + \tau_2) \& (\mathbf{a_y} \geqslant a_c - \tau_2)\} \qquad (27)$$

$$\mathbb{SR}_{\tau_2}^L = \{(\mathbf{a_x}, \mathbf{a_y}) \in \mathbb{SS}_2 | (\mathbf{a_x} \leqslant a_c - \tau_2) \& (\mathbf{a_y} \leqslant a_c + \tau_2)\} \qquad (28)$$

It is acknowledged that the related information of the locality structure can be provided using positive and negative responses. The proposed descriptor splits then, by using the LQP's concept, each quinary pattern into four distinct parts: two negative (i.e., lower) and two positive (i.e., upper) parts to generate four binary codes. With this convention, the four thresholding functions that permit to obtain the two lower and the two upper codes can be expressed in the following ways (cf. Eqs. 29, 30, 31 and 32):

$$\delta_{+1}(\mathbf{a_x}, \mathbf{a_y}) = \begin{cases} 1, & \text{if } (\mathbf{a_x}, \mathbf{a_y}) \in \mathbb{SR}_{\tau_1}^U \\ 0, & \text{otherwise} \end{cases} \qquad (29)$$

$$\delta_{-1}(\mathbf{a_x}, \mathbf{a_y}) = \begin{cases} 1, & \text{if } (\mathbf{a_x}, \mathbf{a_y}) \in \mathbb{SR}_{\tau_1}^L \\ 0, & \text{otherwise} \end{cases} \qquad (30)$$

$$\delta_{+2}(\mathbf{a_x}, \mathbf{a_y}) = \begin{cases} 1, & \text{if } (\mathbf{a_x}, \mathbf{a_y}) \in \mathbb{SR}_{\tau_2}^{U} \\ 0, & \text{otherwise} \end{cases} \quad (31)$$

$$\delta_{-2}(\mathbf{a_x}, \mathbf{a_y}) = \begin{cases} 1, & \text{if } (\mathbf{a_x}, \mathbf{a_y}) \in \mathbb{SR}_{\tau_2}^{L} \\ 0, & \text{otherwise} \end{cases} \quad (32)$$

The local information is encoded using two upper and two lower directional binary dual-cross encoders noted as $E_{\mathbb{SR}_{\tau_1}^{U}}$, $E_{\mathbb{SR}_{\tau_2}^{U}}$, $E_{\mathbb{SR}_{\tau_1}^{L}}$ and $E_{\mathbb{SR}_{\tau_2}^{L}}$ which are based on thresholding functions δ_{+1}, δ_{-1}, δ_{+2} and δ_{-2} and associated to the four sets of pixels relationship $\mathbb{SR}_{\tau_1}^{U}$, $\mathbb{SR}_{\tau_2}^{U}$, $\mathbb{SR}_{\tau_1}^{L}$ and $\mathbb{SR}_{\tau_2}^{L}$, respectively. Formally, the codes produced by the four encoders $E_{\mathbb{SR}_{\tau_1}^{U}}$, $E_{\mathbb{SR}_{\tau_2}^{U}}$, $E_{\mathbb{SR}_{\tau_1}^{L}}$ and $E_{\mathbb{SR}_{\tau_2}^{L}}$ are computed as:

$$E_{\mathbb{SR}_{\tau_1}^{U}}(\mathbf{I}_{m,n}^{3\times3}) = \delta_{+1}(\mathbf{a}_\mu, \mathbf{a}_{\tilde{\mu}}) \times 2^6$$
$$+ \sum_{k=0}^{1} \delta_{+1}(\mathbf{a}_{S_{2k}}, \mathbf{a}_{S_{2k+1}}) \times 2^{5-k}$$
$$+ \sum_{k=0}^{3} \delta_{+1}(\mathbf{a_k}, \mathbf{a_{k+4}}) \times 2^{k} \quad (33)$$

$$E_{\mathbb{SR}_{\tau_1}^{L}}(\mathbf{I}_{m,n}^{3\times3}) = \delta_{-1}(\mathbf{a}_\mu, \mathbf{a}_{\tilde{\mu}}) \times 2^6$$
$$+ \sum_{k=0}^{1} \delta_{-1}(\mathbf{a}_{S_{2k}}, \mathbf{a}_{S_{2k+1}}) \times 2^{5-k}$$
$$+ \sum_{k=0}^{3} \delta_{-1}(a_k, a_{k+4}) \times 2^{k} \quad (34)$$

$$E_{\mathbb{SR}_{\tau_2}^{U}}(\mathbf{I}_{m,n}^{3\times3}) = \delta_{+2}(\mathbf{a}_\mu, \mathbf{a}_{\tilde{\mu}}) \times 2^5$$
$$+ \delta_{+2}(\mathbf{a}_\varrho, \mathbf{a}_{\tilde{\varrho}}) \times 2^4$$
$$+ \sum_{k=0}^{3} \delta_{+2}(a_{2k+1}, \mathbf{a}_{\tilde{S}_k}) \times 2^{k} \quad (35)$$

$$E_{\mathbb{SR}_{\tau_2}^{L}}(\mathbf{I}_{m,n}^{3\times3}) = \delta_{-2}(\mathbf{a}_\mu, \mathbf{a}_{\tilde{\mu}}) \times 2^5 + \delta_{-2}(\mathbf{a}_\varrho, \mathbf{a}_{\tilde{\varrho}}) \times 2^4$$
$$+ \sum_{k=0}^{3} \delta_{-2}(a_{2k+1}, \mathbf{a}_{\tilde{S}_k}) \times 2^{k} \quad (36)$$

- STAGE# 3 (Features extraction): After encoding each pixel in the input texture image using the four directional binary dual-cross encoders $E_{\mathbb{SR}_{\tau_1}^{U}}$, $E_{\mathbb{SR}_{\tau_1}^{L}}$, $E_{\mathbb{SR}_{\tau_2}^{U}}$ and $E_{\mathbb{SR}_{\tau_2}^{L}}$, four code maps are produced. The histograms used as features representing the texture are generated from the obtained four code maps by the following equations:

$$\mathbf{h}_{E_{\mathbb{SR}_{\tau_1}^{U}}}(\mathbf{k}_1) = \sum_{\mathbf{I}_{m,n}^{3\times3}} \widehat{\delta}(E_{\mathbb{SR}_{\tau_1}^{U}}(\mathbf{I}_{m,n}^{3\times3}), \mathbf{k}_1) \quad (37)$$

$$\mathbf{h}_{E_{\mathbb{SR}_{\tau_1}^{L}}}(\mathbf{k}_1) = \sum_{\mathbf{I}_{m,n}^{3\times3}} \widehat{\delta}(E_{\mathbb{SR}_{\tau_1}^{L}}(\mathbf{I}_{m,n}^{3\times3}), \mathbf{k}_1) \quad (38)$$

$$\mathbf{h}_{E_{\mathbb{SR}_{\tau_2}^{U}}}(\mathbf{k}_2) = \sum_{\mathbf{I}_{m,n}^{3\times3}} \widehat{\delta}(E_{\mathbb{SR}_{\tau_2}^{U}}(\mathbf{I}_{m,n}^{3\times3}), \mathbf{k}_2) \quad (39)$$

$$\mathbf{h}_{E_{\mathbb{SR}_{\tau_2}^{L}}}(\mathbf{k}_2) = \sum_{\mathbf{I}_{m,n}^{3\times3}} \widehat{\delta}(E_{\mathbb{SR}_{\tau_2}^{L}}(\mathbf{I}_{m,n}^{3\times3}), \mathbf{k}_2) \quad (40)$$

where $\mathbf{k}_1 \in [0, 2^7]$ is the number of $E_{\mathbb{SR}_{\tau_1}^{U}}$ and $E_{\mathbb{SR}_{\tau_1}^{L}}$ patterns and $\mathbf{k}_2 \in [0, 2^6]$ is the number of $E_{\mathbb{SR}_{\tau_2}^{U}}$ and $E_{\mathbb{SR}_{\tau_2}^{L}}$ patterns. $\widehat{\delta}(\cdot, \cdot)$ denotes the Kronecker delta function defined as below:

$$\widehat{\delta}(\alpha, \beta) = \begin{cases} 1, & \text{if } \alpha = \beta \\ 0, & \text{otherwise} \end{cases} \quad (41)$$

- STAGE #4 (Multi-scale scheme): At present, the histograms from single scale analysis realized with the four directional binary dual-cross encoders $E_{\mathbb{SR}_{\tau_1}^{U}}$, $E_{\mathbb{SR}_{\tau_1}^{L}}$, $E_{\mathbb{SR}_{\tau_2}^{U}}$ and $E_{\mathbb{SR}_{\tau_2}^{L}}$ cannot meet the requirements for ultimate recognition score.

Taking into consideration that various features have various capabilities to demonstrate images and to make them more robust to scale variations, the richer detailed texture information can be captured by multi-scale fusion operation that consists of performing a linear combination of these features. In current study, a novel hybrid histogram is generated by combining the information obtained by $E_{\mathbb{SR}_{\tau_1}^{U}}$, $E_{\mathbb{SR}_{\tau_1}^{L}}$, $E_{\mathbb{SR}_{\tau_2}^{U}}$ and $E_{\mathbb{SR}_{\tau_2}^{L}}$ encoders into a single vector feature. Note that this new hybrid texture description model is expected to be more effective as it permits to reduce the noise sensitivity and improves the discrimination capability of $E_{\mathbb{SR}_{\tau_1}^{U}}$, $E_{\mathbb{SR}_{\tau_1}^{L}}$, $E_{\mathbb{SR}_{\tau_2}^{U}}$ and $E_{\mathbb{SR}_{\tau_2}^{L}}$ operators through their complementary informations. The constructed histogram feature vector of multi-scale analysis is illustrated as follows:

$$\mathbf{h}_{\text{DNT-MQP}} = \left\langle \mathbf{h}_{E_{\mathbb{SR}_{\tau_1}^{U}}}, \mathbf{h}_{E_{\mathbb{SR}_{\tau_1}^{L}}}, \mathbf{h}_{E_{\mathbb{SR}_{\tau_2}^{U}}}, \mathbf{h}_{E_{\mathbb{SR}_{\tau_2}^{L}}} \right\rangle \quad (42)$$

where $\langle \rangle$ is the concatenation operator.

B. PROPOSED DYNAMIC THRESHOLDS FOR DNT-MQP

Evidently, a parametric method evaluated with its user-specified parameters optimized over each tested dataset leads to achieving satisfactory classification results. In this paper, to ensure a meaningful and reasonable comparison with parameter-free state-of-the-arts methods, we propose to define locally and dynamically both parameters τ_1 and τ_2 for quinary pattern creation process of our method. For that, we consider a local image patch of size 3×3 and the neighbor to center difference denoted as $df_{3\times3}$ (cf. Eq. 43) is first calculated. Then, the mean of all negative difference values $df_{3\times3}^{mean^-}$ and the mean of all positive difference values $df_{3\times3}^{mean^+}$ are calculated from the $df_{3\times3}$ set using Eq. 44.

$$df_{3\times3} = [\mathbf{a}_1 - \mathbf{a}_c, \mathbf{a}_2 - \mathbf{a}_c, \dots, \mathbf{a}_7 - \mathbf{a}_c] \quad (43)$$

$$df_{3\times3}^{mean^+} = \frac{1}{pv}\sum_{k=1}^{pv} df_k^+ \qquad df_{3\times3}^{mean^-} = \frac{1}{nv}\sum_{k=1}^{nv} |df_k^-| \quad (44)$$

where df_k^+ and df_k^- are, respectively, the positive (i.e., $\mathbf{a}_k - \mathbf{a}_c \geq 0$) and negative (i.e., $\mathbf{a}_k - \mathbf{a}_c < 0$) difference values in the $df_{3\times3}$ set, pv is the number of df_k^+ elements and nv is the number of df_k^- elements ($pv + nv = $ P). Finally, both parameters τ_1 and τ_2 are measured using the following equation (cf. Eq. 45):

$$\tau_1 = \frac{|df_{3\times3}^{mean^+} - df_{3\times3}^{mean^-}|}{max(df_{3\times3}^{mean^+}, df_{3\times3}^{mean^-})} \quad \tau_2 = \frac{df_{3\times3}^{mean^+} + df_{3\times3}^{mean^-}}{min(df_{3\times3}^{mean^+}, df_{3\times3}^{mean^-})} \quad (45)$$

The pseudo-code of the proposed DNT-MQP descriptor is illustrated in algorithm 1.

C. ADVANTAGES OF DNT-MQP AND DISCUSSION

As a LBP and LQP texture operators variant, the designed DNT-MQP descriptor preserves the same merits concerning the invariance with the monotonic lighting change as well as the low complexity. Furthermore, DNT-MQP presents other merits that are discussed herein below.

Compared to some recent state-of-the-art texture descriptors like LQPAT [47], LCCMSP [49] and ARCSLBP [63], which suffer from an inborn defect of LBP, DNT-MQP descriptor can better describe local texture characteristics of the image with lower computational complexity. In order to visually show the effectiveness of the coding strategy of DNT-MQP, we illustrate in Figure 3 examples of histogram based-matching of two sample texture images, selected from USPTex database and belonging to two distinct texture classes using DNT-MQP, LQPAT, LCCMSP and ARCSLBP. It is easy to observe that DNT-MQP carries more information than those of the other descriptors which permit to DNT-MQP to have better discriminative ability compared to LQPAT, LCCMSP and ARCSLBP. Moreover, the histograms of both images using DNT-MQP are considered as not similar since the distance (using L1-city block distance) between the two samples, which is 1.1298 is higher compared to LQPAT, LCCMSP and ARCSLBP where their measured distances which are respectively 0.6173, 0.6924 and 0.7119, can be considered similar (lower than those obtained by DNT-MQP). To further highlight its effectiveness, DNT-MQP is applied on various challenging representative texture datasets in the Section IV.

IV. EXPERIMENTAL RESULTS AND DISCUSSION

In this phase of study, we show the effectiveness and validate the performance stability of the proposed DNT-MQP operator with comprehensive tests on sixteen representative widely used texture databases. Furthermore, DNT-MQP is compared to a large number of recent most promising state-of-the-art texture descriptors and several CNN-based features to highlight its provided performance improvement. The evaluated methods are summarized in Table 1. Note that, some of these methods are implemented using the original available codes while for the others we have used our own implementation according to their respective papers and which are fine tuned

---

Algorithm 1 Computing DNT-MQP descriptor

Require: $I \leftarrow$ input grayscale image $I_{M\times N}$.
Output: $\mathbf{h}_{\text{DNT-MQP}} \leftarrow$ the multi-scale histogram feature.
1: Calculate the average global gray levels $\mathbf{a}_{\widetilde{\mu}}$ of the whole image $I_{M\times N}$ using Eq. 19
2: Calculate the median of the grey-scale values $\mathbf{a}_{\widetilde{\varrho}}$ of the whole image $I_{M\times N}$.
3: **for** Each image pixel $\mathbf{a}_c$ of $I_{M\times N}$ **do**
4:     Consider a local square window $\mathbf{I}_{m,n}^{3\times3}$ of dimension 3×3 around $\mathbf{a}_c$.
5:     Calculate the neighbor to center difference $df_{3\times3}$ and then calculate both dynamic thresholds τ_1 and τ_2 using Eq. 45.
6:     Calculate the average directional gray levels $\mathbf{a}_{S_k}$ and $\mathbf{a}_{\widetilde{S}_k}$ according to both sets S_k and $\widetilde{S}_k$ (cf. Eqs 16 and 17) using Eqs. 20 and 21.
7:     Calculate (using Eqs. 33, 34, 35 and 36, respectively):
- $E_{\mathbb{SR}_{\tau_1}^U}(\mathbf{I}_{m,n}^{3\times3}) \leftarrow$ the upper directional binary code based on thresholding function δ_{+1} and associated to the set of pixels relationship $\mathbb{SR}_{\tau_1}^U$.
- $E_{\mathbb{SR}_{\tau_1}^L}(\mathbf{I}_{m,n}^{3\times3}) \leftarrow$ the lower directional binary code based on thresholding function δ_{-1} and associated to the set of pixels relationship $\mathbb{SR}_{\tau_1}^L$.
- $E_{\mathbb{SR}_{\tau_2}^U}(\mathbf{I}_{m,n}^{3\times3}) \leftarrow$ the upper directional binary code based on thresholding function δ_{+2} and associated to the set of pixels relationship $\mathbb{SR}_{\tau_2}^U$.
- $E_{\mathbb{SR}_{\tau_2}^L}(\mathbf{I}_{m,n}^{3\times3}) \leftarrow$ the lower directional binary code based on thresholding function δ_{-2} and associated to the set of pixels relationship $\mathbb{SR}_{\tau_2}^L$.
8: **end for**
9: Calculate (using Eqs. 37, 38, 39 and 40, respectively):
- $\mathbf{h}_{E_{\mathbb{SR}_{\tau_1}^U}} \leftarrow$ histogram feature of $E_{\mathbb{SR}_{\tau_1}^U}$ code map.
- $\mathbf{h}_{E_{\mathbb{SR}_{\tau_1}^L}} \leftarrow$ histogram feature of $E_{\mathbb{SR}_{\tau_1}^L}$ code map.
- $\mathbf{h}_{E_{\mathbb{SR}_{\tau_2}^U}} \leftarrow$ histogram feature of $E_{\mathbb{SR}_{\tau_2}^U}$ code map.
- $\mathbf{h}_{E_{\mathbb{SR}_{\tau_2}^L}} \leftarrow$ histogram feature of $E_{\mathbb{SR}_{\tau_2}^L}$ code map.
10: Calculate the multi-scale histogram feature $\mathbf{h}_{\text{DNT-MQP}}$ using Eq. 42.
11: **return** $\mathbf{h}_{\text{DNT-MQP}}$

---

to get the same output results as given in the published paper. The experiments herein follow the standard evaluation protocol for each tested dataset (i.e., split-sample validation) where 50% of the samples are randomly selected to be used as the training set, and the remaining 50% of the samples are regarded as the testing set. The samples of the test set are then classified through the parameter-free nearest-neighbor rule (1-NN) with L1-city block distance. We repeat each experiment 100 times to remove any bias related to the division of the dataset and the averaged results are considered as estimated accuracies. In what follows, the texture datasets
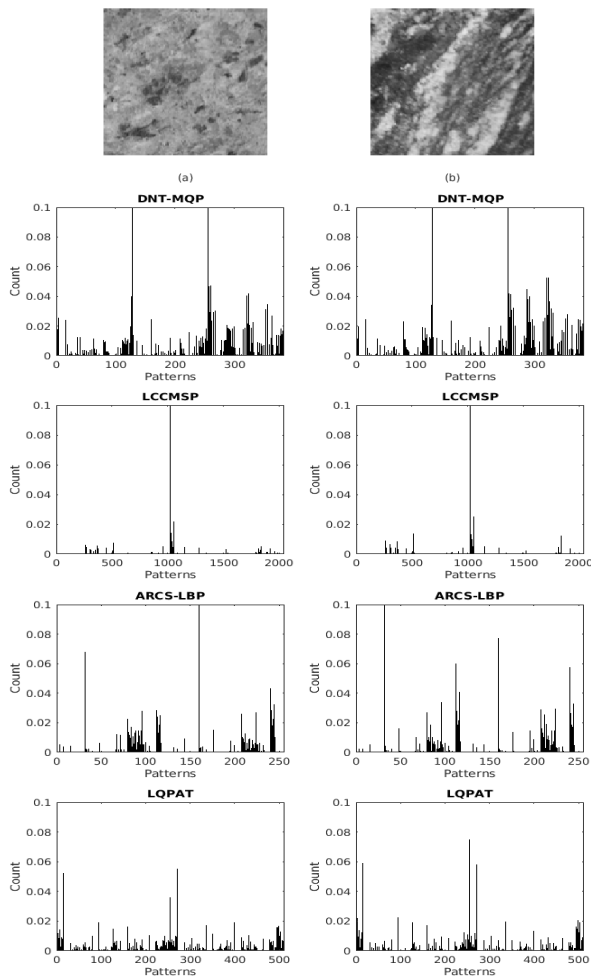
FIGURE 3. Comparison of DNT-MQP, LCCMSP, ARCSLBP and LQPAT features on two sample texture images representing two distinct texture classes from USPTex dataset, left and right columns present, respectively, the histograms of the images (a) and (b) using the different descriptors.

TABLE 1. Texture descriptors tested and compared with our proposed descriptor.

| Name	Acronym	Ref.
Local contrast patterns	LCP	[41]
Space-frequency co-occurrences via local quantized patterns	GLR	[42]
Deep Convolutional Neural Networks	AlexNet	[43]
Visual Geometry Group	VGG16	[44]
Visual Geometry Group	VGG19	[44]
Deep residual learning for image recognition	ResNet-50	[45]
Deep residual learning for image recognition	ResNet-101	[45]
Median robust extended local binary pattern	MRELBP	[46]
Statistical binary patterns	SBP	[27]
Local quadruple pattern	LQPAT	[47]
Locally encoded transform feature histogram	LETRIST	[65]
Local neighborhood difference pattern	LNDP	[48]
Centre symmetric quadruple pattern	CSQP	[51]
Local directional ZigZag pattern	LDZP	[26]
Mixed neighborhood topology cross decoded patterns	MNTCDP	[56]
Local directional ternary pattern	LDTP	[57]
Local neighborhood intensity pattern	LNIP	[25]
Local diagonal extrema number pattern	LDENP	[30]
Local concave-and-convex micro-structure patterns	LCCMSP	[49]
Local optimal-oriented pattern	LOOP	[29]
Repulsive-and-attractive local binary gradient contours	RALBGC	[52]
Local directional edge binary patterns	LDEBP	[28]
Directional coding	DC	[31]
Local directional value	LDV	[32]
Attractive-and-repulsive center-symmetric LBP	ARCSLBP	[63]
Multi kernel based local binary pattern	KLBP	[33]
Cascaded asymmetric local pattern	CALP	[34]
Improved local quinary patterns	ILQP	[35]
Elliptical upper and lower local ternary pattern	EUL_{LTP}	[36]
Multi-direction local binary pattern	MDLBP	[64]
R-theta local neighborhood pattern	RTLNP	[67]
Adaptive curvelets	AC	[68]
Local grouped order pattern and non-local binary pattern	LGONBP	[69]
Spatio-spectral network	SSN	[70]

has its own specific challenges in terms of rotation, scale, translation, illumination, view angle and other variations, which will allow the performance of the proposed descriptor as well as those of the evaluated state-of-the-art methods to be assessed against these factors.

B. EFFECTS OF DIFFERENT COMPONENT COMBINATIONS

Generally, it is difficult to fulfill simultaneously several qualities by a single encoder. The trend towards combining several texture representations generated using different encoders seems to be the best way forward. Indeed, the combination can be suitable in order to exploit advantages of each encoders, reduce the problems that arise in each individual method and, then, improve the classification results. There are four main components in the designed DNT-MQP descriptor, such as $E_{\mathbb{SR}_{\tau_1}^U}$, $E_{\mathbb{SR}_{\tau_1}^L}$, $E_{\mathbb{SR}_{\tau_2}^U}$ and $E_{\mathbb{SR}_{\tau_2}^L}$ (denoted as single scale DNT-QP1, DNT-QP2, DNT-QP3, DNT-QP4, respectively in Figure 4) encoders where their combination gives rise to the DNT-MQP descriptor (DNT-MQP=⟨DNT-QP1, DNT-QP2, DNT-QP3, DNT-QP4⟩). In this subsection, we evaluate their effects and impact on the overall performance applied alone, in combination two by two (DNT-QP12=⟨DNT-QP1, DNT-QP2⟩ and DNT-QP34= ⟨DNT-QP3, DNT-QP4⟩), three by three (DNT-QP123 = ⟨DNT-QP1, DNT-QP2, DNT-QP3⟩ and DNT-QP124 = ⟨DNT-QP1, DNT-QP2, DNT-QP4⟩) against the DNT-MQP descriptor using the USPtex, MondialMarmi and NewBarkTex databases. It can be seen from Figure 4 that the classification accuracy has improved every time a new component is added, demonstrating the effectiveness of each component and thus justifying the fact of combining the different components. The DNT-MQP descriptor which is an hybrid texture description model that combines all the four components achieves the best classification results as

considered in the experiments are first presented and the obtained experimental results are then discussed.

A. TEXTURE DATASETS

For the sake of verification of the effectiveness and performance stability of DNT-MQP, we carried out extensive tests on sixteen well-known texture databases including Jerry Wu, CUReT, KTH-TIPS, USPTex, Brodatz, KTH-TIPS2b, Bonn BTF, MondialMarmi, TC-00, TC-01, TC-13, Kylberg and XUH databases (the same datasets used in [52], [63]), New-BarkTex[1] and MBT[2] databases. These well-known datasets for texture classification (recognition) were selected to cover various characteristics in terms of number of samples, number of classes and specific challenges posed by each texture dataset. More information about each dataset is summarized in Table 2. As can be seen from Table 2, each texture dataset

[1] https://www-lisic.univ-littoral.fr/~porebski/BarkTex_image_test_suite.html

[2] https://multibandtexture.recherche.usherbrooke.ca/multi-band.html

TABLE 2. Image datasets used in this study. The Table presents the properties of each dataset, including the number of classes and variety of samples in view point, scale, illumination changes, rotation, etc.

No.	Name	Classes	Total samples	Challenges
1	USPtex	191	2292	Real-world texture images acquired in the wild which are obtained by photographing natural objects and landscapes using different conditions for lighting, geometrical positioning, noise, et.
2	Brodatz	13	208	Images are not acquired under controlled conditions or corrected in any way and there is a lack of intraclass variations.
3	KTH-TIPS2b	11	176	Images acquired under illumination, rotation, pose and scale changes.
4	MondialMarmi	12	768	Images acquired under controlled illumination conditions. The dataset includes hardware and software-rotated images.
5	TC-00	24	480	Images acquired under controlled and variable conditions of illumination, rotation and spatial resolution.
6	TC-01	24	2112	Some properties as TC-00.
7	TC-13	68	1360	Images acquired under invariable illumination, rotation and scale.
8	CUReT	61	5612	Images present wide variety of geometric and photometric properties as intra-class variations in rotation, illumination, and viewing angle.
9	KTH-TIPS	10	40	Images captured under nine scales, nine illumination conditions and three poses.
10	NewBarkTex	6	1632	Images characterize the natural color textures acquired under natural illumination conditions.
11	Jerry Wu	39	156	Images acquired under different combinations of illumination direction, imaging direction and surface rotation.
12	Bonn BTF	10	160	Images acquired under varying viewing and illumination angle.
13	XUH	25	1000	Images acquired under under different rotation angles, different viewpoints, and different illuminations.
14	Kylberg	28	4480	Images acquired under controlled illumination conditions and corrected for lens distortion, chromatic aberration and vignetting.
15	MBT	154	2464	Images have high spatial resolution, which are common in areas such as astronomy and remote sensing.
16	UMD	25	1000	Images acquired under small illumination changes, strong scale, rotation and viewpoint changes.
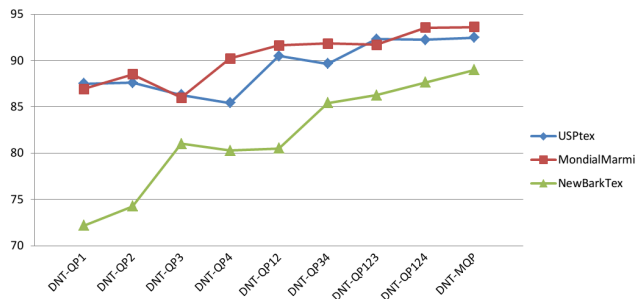
FIGURE 4. Classification results of single-scale image descriptors with their combinations.

it extracts complementary texture information from fused components.

C. COMPARATIVE ASSESSMENT OF PERFORMANCE

1) EXPERIMENT #1: INVESTIGATION ON PERFORMANCE STABILITY

Table 3 depicts the average classification scores (i.e., over the 100 subdivisions) of each tested method and for each texture database as well as the global average performance (GAP) and the mean of standard deviation (mean Std) of each method over all the datasets. According to the results reported in Table 3, we can readily make the following observations:

- It is easy to observe that descriptors like LDENP, LDV, DC and EUL_{LTP} present the lowest performance on almost all the used dataset. Indeed, these methods are often found at the bottom of the ranking as they achieve classification performance which are mostly poor or at least lowest than the other evaluated descriptors.

- Results indicate that, except operators like LDENP, LDV, DC and EUL_{LTP} which perform poorly, all the other evaluated methods show promising results on Brodatz database (dataset 2 in Table 3) where their

achieved score are above 96%. Descriptors like LDZP, KLBP, ILQP, RALBGC, LCCMSP, ARCS-LBP, LDTP, MNTCDP as well as the designed DNT-MQP operator manage to differentiate all classes perfectly (score equal to 100%) on Brodatz database, leaving then essentially no room for improvement. This remark is also true for KTH-TIPS database (dataset 9 in Table 3) where DNT-MQP as well as several evaluated state-of-the-art descriptors manage to differentiate all classes perfectly.

- It can be found that there is a notable performance drop for all the tested operators on several datasets including USPtex, MondialMarmi, KTH-TIPS2b, TC-13, New-BarkTex and MBT (datasets 1, 3, 4, 7, 10, 13, and 16 in Table 3). The overall classification accuracy achieved on TC-13, NewBarkTex and MBT are below 90%. It is worth mentioning that in this study the 1-NN classifier was used for classification but more complicated machine learning algorithms such as support vector machine (SVM) and extended nearest neighbor (ENN) may improve the overall performance.

- It is evident from the results reported in Table 3 that none of the evaluated methods ensure obtaining satisfactory classification results over all the sixteen tested datasets. Considering for example the DC descriptor, it performs nicely on Brodatz, KTH-TIPS (it gets a score of 100%) and Kylberg datasets but shows poor performance on the others tested datasets. We can express the same remark for many other evaluated methods. LETRIST descriptor which is ranked as the 4th best descriptor as will be shown later, it allows achieving good classification results on the majority of the considered datasets but its weaknesses appeared in classifying the images of the NewBarkTex dataset as the achieved score drops dramatically and is about 63% vs 86.98% (difference of around 23.86%) realized with the top 1 descriptor

TABLE 3. Average classification accuracy. The last two columns represent, respectively, the global average performance (GAP) and the mean standard deviation of each method over all the datasets. The SSN operator as a color image descriptor is only evaluated on color texture datasets.

Texture descriptor	Dataset 1	2	3	4	5	6	7	8	9	10	11	12	13	14	15	16	GAP	mean Std
DNT-MQP	92.46	100	95.12	93.64	99.97	99.7	86.59	95.52	100	88.97	99.9	99.25	98.11	99.92	86.91	98.55	95.91	0.61
SBP2	89.28	99.92	90.89	89.71	98.91	97.65	84.24	96.45	99.45	64.56	98.74	99.91	98.4	99.71	76.63	98.53	92.68	0.85
LETRIST	89.34	99.99	90.08	86.99	99.92	98.51	83.65	98	100	69.36	100	100	97.99	99.86	81.39	98.51	93.34	0.7
LCCMSP	88.42	100	93.32	90.79	99.97	99.68	84.44	94.45	100	84.8	98.18	97.64	96.64	99.69	85.41	96.96	94.39	0.78
MDLBP	69.47	99.23	77.99	76.33	99.63	97.12	74.77	81.26	99.6	64.22	94.55	96.45	88.29	97.04	72.93	91.83	86.29	1.26
LOOP	79.47	99.97	85.81	79.27	99.49	97.83	76.48	90.61	100	70.22	96.86	98.78	91.05	97.75	83.99	94.3	90.11	0.95
LDEBP	84.85	99.96	87.3	82.7	99.27	98.19	80.66	89.33	100	71.2	98.87	92.96	93.17	98.8	84.15	95.7	91.06	0.94
ARCS-LBP	86.89	99.88	93.23	90.86	99.65	99.31	85.29	94.03	100	79.66	99.53	99.17	97.23	99.8	83.23	97.52	94.08	0.78
LDENP	44.99	95.4	65.8	57.8	95.12	81.66	63.61	64.61	88.8	52.45	88.5	88.29	69.27	87.13	60.4	78.09	73.87	1.87
LDTP	83	100	90.47	85.97	99.76	99.2	80.32	91.54	100	72.3	98.23	99.88	91.54	97.74	82.97	94.49	91.71	0.80
LDZP	70.51	100	88.53	83.02	99.48	97.77	80.28	84.84	99.75	67.28	96.72	96.85	84.01	92.5	84.18	88.89	87.74	1.13
DC	61.09	99.48	79.78	67.35	92.91	88.13	68.29	80.67	100	49.63	94.95	93.36	91.07	97.92	56.24	93.41	82.14	1.18
LDV	44.71	98.68	68.57	43.63	95.68	84.01	59.41	92.55	89.95	48.16	94.71	98.04	88.9	98.76	61.95	87.75	78.46	1.50
KLBP	85.07	100	91.24	86.54	99.54	99.19	79.9	91.12	100	79.04	97.49	97.34	92.55	98.6	86.78	95.25	92.47	0.89
LNIP	76.48	99.73	82.97	82.86	99.02	98.14	76.1	85.88	98.45	65.93	96.86	77.86	89.18	96.55	83.99	92.04	87.62	1.22
CALP	75	99.4	82.63	75.28	98.99	96.41	76.44	92.39	98.15	72.55	95.76	95.83	89.68	98.72	84.3	91.05	88.91	1.29
ILQP	87.54	100	93.39	90.04	99.63	99.32	80.12	91.03	100	82.35	98.03	98.72	92.14	98.33	85.8	96.67	93.31	0.82
EULLTP	64.95	99.38	78.63	69.31	96.68	90.92	66.91	73.35	93.9	71.32	92.58	93.4	82.43	94.87	71.75	88.61	83.06	1.46
MRELBP	84.38	100	89	84.17	99.54	97.56	81.39	96.24	100	59.56	99.53	98.97	99.01	99.01	75.66	88.96	91.49	0.79
MNTCDP	85.73	100	90.93	91.67	99.93	99.57	82.97	92.4	100	70.59	100	100	94.91	98.48	78.95	95.42	92.59	0.71
LNDP	80.18	99.97	88.72	80.73	99.48	96.85	75.97	91.12	100	73.28	97.44	93.85	90.16	97.89	87.49	93.8	90.43	1.00
LQPAT	77.13	99.93	83.76	81.58	99.81	97.67	76.89	90.46	99.6	75	97.28	94.94	89.2	96.92	84.73	92.04	89.80	1.10
CSQP	72.61	99.93	80.12	74.81	99.1	96.92	74.9	88.24	100	69.61	98.42	95.26	88.94	96.87	81.84	90.39	87.99	1.02
RALBGC	87.16	100	93.39	89.2	99.9	99.15	83.86	93.31	100	84.31	97.51	98.8	95.69	99.09	86.22	96.42	94.00	0.80
LGONBP	79	99.84	85.51	85.2	99.31	97.28	81.21	97.21	100	60.78	99.35	99.28	98.16	99.85	72.31	98.07	90.77	0.91
AC	74.23	99.97	89.14	87.26	96.89	94.49	83.72	88.46	98.6	76.47	88.95	99.96	87.38	89.55	63.17	88.29	87.90	1.29
RTLNP	47.68	97.55	65.19	51.09	95.34	87.48	53.03	80.25	88.5	55.51	83.72	93.94	86.63	98.73	62.95	86.71	75.26	1.71
LCP	63.91	99.83	81.59	74.67	97.56	91.72	74.39	94.56	96.50	53.19	99.14	97.17	96.89	99.67	68.76	96.97	86.65	1.21
GLR	88.08	100.00	87.70	85.98	99.77	97.77	82.84	98.53	100.00	58.82	100.00	98.51	98.39	99.84	80.25	98.49	92.18	0.77
SSN	88.50	-	-	-	-	-	86.55	-	-	70.83	-	-	-	-	46.6	-	73.12	1.99

(i.e., the proposed DNT-MQP descriptor). The same comment is true for many other methods such as CSQP, LOOP, LDEBP and so on.

- It can also be seen in Table 3 that DNT-MQP realizes a performance that is competitive or better than all the evaluated state-of-the-art descriptors. Furthermore, according to literature review it can be found that DNT-MQP universally is among one of the best descriptors in terms of overall accuracy as it achieves outstanding classification outcomes on nearly all the selected datasets. The striking performance of DNT-MQP can be judged by the fact that it realizes the highest global average performance (GAP) against all the evaluated methods.

- Remarkably, DNT-MQP achieves superior classification results against SSN (Spatio-Spectral Networks) descriptor, which was originally designed for color-texture analysis, on USPtex, TC-13, NewBarkTex and MBT color texture datasets. The SSN method, like the majority of the methods oriented to color texture analysis, tends to be more sensitive to illumination and resolution [71]. Also, it chiefly either does not consider spatial relationships between the pixels in the image or give lower weightages. Thereby, dominant color gives the distribution of the features, which may lead to lower accuracy. While, DNT-MQP has several advantages, including invariance with the monotonic lighting change, low complexity and low-dimensionality in feature representation.

- Noticeably, considering the ranking between the tested descriptors within each used dataset, DNT-MQP stands out as the best descriptor as it performs consistently and significantly the best for ten texture

datasets: USPtex, Brodatz, KTH-TIPS2b, Mondial-Marmi, TC-00, TC-01, TC-13, KTH-TIPS, NewBarkTex and Kylberg datasets (1-7, 9, 10, and 15, respectively). Furthermore, it is in the top 3 methods on four tested datasets. It is interesting to note that when DNT-MQP does not achieve the highest specific scores (i.e., it is not the top texture descriptor), it provides an interesting competitive average performance compared to the score yielded by the top one texture operator. Considering for example Bonn BTF dataset (number 12) where DNT-MQP has the sixth-highest average performance (i.e., ranked at the 6th position), it allowed to reach a score of 99.25% which is considered as very satisfactory classification result (very close to the score of the descriptors ranked before it: 100% for the top one).

- The outstanding results on KTH-TIPS2b, Mondial-Marmi, TC-00, TC-01, TC-13, Jerry Wu and UMD verify the fact that DNT-MQP can resist the rotation variations. Note that DNT-MQP has good tolerance to rotation against LETRIST and SBP2 which are originally conceived/developped for rotation-invariant texture classification. In particular, DNT-MQP achieves 95.12%, 93.64%, 99.70%, 86.59% on KTH-TIPS2b, MondialMarmi, TC-01 and TC-13, respectively, where the performance improvement over SBP2 and LETRIST on these datasets are of (4.23%,5.04%), (3.93%,6.65%), (2.05%, 1.19%) and (2.35%, 2.94%). Furthermore, DNT-MQP has good tolerance to illumination changes as it provides the best average performance on KTH-TIPS2b, TC-00, TC-01, TC-13, KTH-TIPS, NewBark-Tex and UMD datasets and interesting competitive classification results on CUReT, Jerry Wu, Bonn BTF and Kylberg datasets. In addition, the obtained superior and

or competitive satisfactory results on, on the one side, UMD, TC-13 and KTH-TIPS2b, and on, on the other side, UMD and XUH, indicate that DNT-MQP has good tolerance to scale changes and viewpoint changes, respectively.

Considering the above discussions, it can be noticed that the designed DNT-MQP operator shows a significant performance stability over the evaluated state-of-the-art texture methods on almost all the considered datasets. Indeed, DNT-MQP has lower oscillation of performance as it keeps a consistent performance throughout various texture databases while most of the literature methods oscillate. The performance stability can also be confirmed by the fact that DNT-MQP has achieved the lowest mean standard deviation, corroborating to its robustness against any bias related to the division of the datasets. These indicate that the combination of single scale DNT-QP features helped to construct a texture operator that performs better on a wide selection of various texture datasets.

2) EXPERIMENT #2: STATISTICAL SIGNIFICANCE OF THE OBTAINED RESULTS IN TERMS OF ACCURACY IMPROVEMENT

The major reason to carry out this experiment is to further validate statistically the obtained classification results via the designed method vs the evaluated state-of-the-art descriptors using the Wilcoxon signed rank test based ranking technique proposed in [49]. The technique is applied on all the pairwise combinations of the 24 evaluated texture descriptors considered in this experiment on the sixteen used texture datasets. Table 4 gathers the obtained ranking results according to the normalized number of victories (number of wins/(number of tested datasets*(number of tested descriptors - 1))) achieved by each evaluated method on all the tested datasets. It is easy to observe from the results shown in Table 4 that the designed DNT-MQP operator is clearly the best performing descriptor in comparison with the evaluated state-of-the-art methods, which corroborate all the result analysis extracted from Table 3. Remarkably, the normalized number of victories achieved by DNT-MQP is 0.80, vs. 0.71 with LETRIST (top 2nd), vs. 0.68 with LCCMSP (top 3th), vs. 0.67 with ARCS-LBP (top 4th), etc. Particularly, if we consider the classification performance of LETRIST (the best second descriptor) as baseline, DNT-MQP texture operator provides about 11.5% improvement over the sixteen tested texture datasets.

3) EXPERIMENT #3: COMPARISONS WITH CNN-BASED FEATURES

To evaluate in depth the effectiveness of DNT-MQP at the highest level, we also compared its performance to that of the well-known CNN-based features using the pre-trained deep learning models ResNet50, ResNet101, AlexNet, VGG16 and VGG 19, with varying layers in some of them. Note that the outputs of the evaluated CNN-based features are treated as feature vectors that are exploited in a manner similar to how handcrafted features are normally

TABLE 4. Ranking outcomes based on the normalized number of victories achieved by each applied method on all the used datasets after applying the Wilcoxon-based ranking test.

Ranking 1-NN	Texture descriptor	Victories/comparisons	Dimension
1	DNT-MQP	0.80134	384
2	LETRIST	0.71875	413
3	LCCMSP	0.68750	2046
4	ARCS-LBP	0.67188	256
5	GLR	0.64286	1728
6	RALBGC	0.64062	1022
7	MNTCDP	0.63839	2048
8	SBP2	0.60938	400
9	MRELBP	0.60714	800
10	ILQP	0.58929	1024
11	LGONBP	0.54911	1404
12	LDTP	0.53348	1022
13	KLBP	0.53125	1280
14	LDEBP	0.46652	64
15	LNDP	0.40625	256
16	LOOP	0.40402	256
17	LQPAT	0.36830	512
18	LCP	0.36384	171
19	CALP	0.31473	192
20	AC	0.30357	376
21	LDZP	0.29464	354
22	LNIP	0.28795	512
23	CSQP	0.27232	256
24	MDLBP	0.24330	256
25	DC	0.16964	225
26	LDV	0.16071	512
27	EULLTP	0.10938	32
28	RTLNP	0.06920	1024
29	LDENP	0.02009	15

used. Table 5 summarizes the comparison results. Noticeably, it can be found that DNT-MQP reaches the highest average performance compared, similarly to the local descriptors, to all tested CNN-based features on 10 datasets out of 16. Note that, when DNT-MQP is not ranked at the first position, it allowed, as shown in Table 5, to provide an interesting average performance, although not achieving the highest specific scores (i.e., it achieves similar accuracies to the CNNs ranked before it), but with the advantage of DNT-MQP being conceptually much easier to implement and training free. Note that CNNs are more suitable when there is high intraclass variability, whereas local descriptors works better with homogeneous, fine-grained textures with low intraclass variability. Indeed, when the images have similar contents and fewer patterns, the deep models tend to extract redundant feature values which make the classifier perform badly on these features and make different models provide nearly the same performance. On the other hand, when the images have complex contents and various patterns, like in the USPtex dataset, the deep features provide better presentation than the local descriptors [70].

D. RESEARCH IMPLEMENTATION

A laptop, equipped with a 2.10 GHz Core i7 CPU, 8 GB of RAM and having Ubuntu 14.04 trusty operating system was used in the experiments. We implemented all the methods using MATLAB R2013a. The implementation of the used methods needed approximately 97 hours. Figure 5 demonstrates the required time for processing (in minutes) containing time for feature extraction, calculation of distance and also 1-NN classification applied to 23940 images in the 16 datasets used in this study. According to Figure 5, it can be seen that the proposed DNT-MQP method is faster than the two best performing descriptors ranked after it which

TABLE 5. Performance comparison of DNT-MQP and CNN-based features. The last column represent the global average performance (GAP) of each method over all the datasets.

| Methods	Dataset																GAP
	1	2	3	4	5	6	7	8	9	10	11	12	13	14	15	16	
DNT-MQP	92.46	100	95.12	93.64	99.97	99.7	86.59	95.52	100	88.97	99.9	99.25	98.11	99.92	86.91	98.55	95.91
resnet50	95.84	99.3	90.44	77.94	99.56	97.29	82.82	96.91	92.6	79.31	98.71	94.35	98.78	99.89	88.23	98.73	93.16
resnet101	94.97	98.78	87.1	80.68	99.28	97.71	83.17	96.99	93.75	79.79	98.4	94.52	98.89	99.87	86.27	98.94	93.06
vgg19–Fc7	96.07	100	94.3	81.85	99.51	98.47	83.67	95.04	100	80.02	98.83	98.57	98.12	99.71	81.91	98.05	94.00
vgg19–Fc6	95.78	100	94.78	83.21	99.81	98.51	83.47	96.3	100	80.86	99.18	98.84	97.97	99.79	81.93	97.99	94.27
vgg16–Fc7	95.79	99.99	94.15	82.94	99.69	98.31	84.42	95.97	100	78.15	99.58	99.57	99.03	99.59	83	98.99	94.32
vgg16–Fc6	95.73	99.98	93.85	82.69	99.95	98.38	84.85	96.64	100	78.91	99.9	99.04	98.75	99.71	84.05	98.66	94.44
alexnet–Fc7	95.31	99.14	90.18	81.17	98.92	97.99	82.7	95.32	99.7	78.42	97.51	99.47	96.43	98.63	79.34	96.5	92.92
alexnet–Fc6	95.35	99.99	91	82.07	99.42	98.62	83.15	96.72	100	80.59	99.31	99.16	96.36	98.99	79.76	96.35	93.55
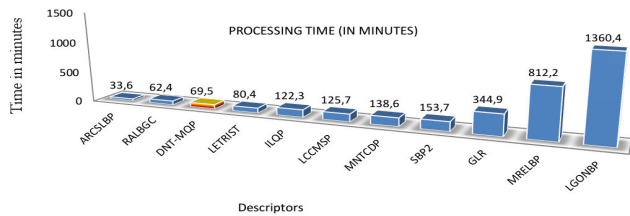
FIGURE 5. Processing time (in minutes) of the top twelve tested texture descriptors over all considered dataset.

confirms that DNT-MQP makes an admissible tradeoff between speed and classification performance.

V. CONCLUSION

Herein, motivated by several state-of-the-art LBP-like methods, a conceptually simple, easy-to-implement yet highly discriminative texture operator so-called Directional Neighborhood Topologies based Multi-scale Quinary Pattern (DNT-MQP) is designed for texture description and classification. DNT-MQP operator captures, thanks to the use of several directional neighborhood topologies, richer detailed and complementary texture information. As it has been proved through the experimental results, DNT-MQP showed its high ability to differentiate, with high precision, different classes of a great number of benchmark texture datasets, while enjoying a low-dimensional representation. Furthermore, the discriminative power of DNT-MQP is proved against 34 recent state-of-the-art methods, indicating that DNT-MQP is a strong candidate for texture modeling. Future work will concern the investigation of the use of other well known classifiers to increase classification performance of the proposed model. In addition, the proposed texture operator holds potential for deployment across high-level challenging applications related to texture classification including dynamic texture classification, background subtraction in complex scenes, object recognition and video-based face analysis and so on.

REFERENCES

[1] D. Hong, W. Liu, J. Su, Z. Pan, and G. Wang, "A novel hierarchical approach for multispectral palmprint recognition," *Neurocomputing*, vol. 151, pp. 511–521, Mar. 2015.

[2] D. Hong, X. Wu, P. Ghamisi, J. Chanussot, N. Yokoya, and X. X. Zhu, "Invariant attribute profiles: A spatial-frequency joint feature extractor for hyperspectral image classification," *IEEE Trans. Geosci. Remote Sens.*, vol. 58, no. 6, pp. 3791–3808, Jun. 2020.

[3] L. Liu, J. Chen, P. Fieguth, G. Zhao, R. Chellappa, and M. Pietikäinen, "From BoW to CNN: Two decades of texture representation for texture classification," *Int. J. Comput. Vis.*, vol. 127, no. 1, pp. 74–109, Jan. 2019.

[4] L. Armi and S. Fekri-Ershad, "Texture image analysis and texture classification methods—A review," 2019, *arXiv:1904.06554*. [Online]. Available: http://arxiv.org/abs/1904.06554

[5] M. Kas, Y. El-merabet, Y. Ruichek, and R. Messoussi, "A comprehensive comparative study of handcrafted methods for face recognition LBP-like and non LBP operators," *Multimedia Tools Appl.*, vol. 79, pp. 1–39, Aug. 2019.

[6] B. S. Manjunath and W. Y. Ma, "Texture features for browsing and retrieval of image data," *IEEE Trans. Pattern Anal. Mach. Intell.*, vol. 18, no. 8, pp. 837–842, Aug. 1996.

[7] L. S. Davis, "Polarograms: A new tool for image texture analysis," *Pattern Recognit.*, vol. 13, no. 3, pp. 219–223, Jan. 1981.

[8] T. Ojala, M. Pietikäinen, and D. Harwood, "A comparative study of texture measures with classification based on featured distributions," *Pattern Recognit.*, vol. 29, no. 1, pp. 51–59, Jan. 1996.

[9] J. Duvernoy, "Optical–digital processing of directional terrain textures invariant under translation, rotation, and change of scale," *Appl. Opt.*, vol. 23, no. 6, pp. 828–837, 1984.

[10] R. K. Goyal, W. L. Goh, and D. P. Mitaletal, "Scale and rotation invariant texture analysis based on structural property," in *Proc. IEEE Int. Conf. Ind. Electron., Control, Instrum.*, Nov. 1995, pp. 1290–1294.

[11] G. Eichmann and T. Kasparis, "Topologically invariant texture descriptors," *Comput. Vis., Graph., Image Process.*, vol. 41, no. 3, pp. 267–281, Mar. 1988.

[12] R. L. Kashyap and A. Khotanzad, "A model-based method for rotation invariant texture classification," *IEEE Trans. Pattern Anal. Mach. Intell.*, vol. PAMI-8, no. 4, pp. 472–481, Jul. 1986.

[13] F. S. Cohen, Z. Fan, and M. A. Patel, "Classification of rotated and scaled textured images using Gaussian Markov random field models," *IEEE Trans. Pattern Anal. Mach. Intell.*, vol. 13, no. 2, pp. 192–202, Feb. 1991.

[14] R. Porter and N. Canagarajah, "Robust rotation invariant texture classification," in *Proc. IEEE Int. Conf. Acoust., Speech, Signal Process.*, Apr. 1997, pp. 3157–3160.

[15] L. Liu and P. Fieguth, "Texture classification from random features," *IEEE Trans. Pattern Anal. Mach. Intell.*, vol. 34, no. 3, pp. 574–586, Mar. 2012.

[16] A. Fernández, "Robust color texture features based on ranklets and discrete Fourier transform," *J. Electron. Imag.*, vol. 18, no. 4, Oct. 2009, Art. no. 043012.

[17] L. Nanni, A. Lumini, and S. Brahnam, "Local binary patterns variants as texture descriptors for medical image analysis," *Artif. Intell. Med.*, vol. 49, no. 2, pp. 117–125, Jun. 2010.

[18] M. Varma and A. Zisserman, "A statistical approach to material classification using image patch exemplars," *IEEE Trans. Pattern Anal. Mach. Intell.*, vol. 31, no. 11, pp. 2032–2047, Nov. 2009.

[19] Y. Xu, H. Ji, and C. Fermuller, "A projective invariant for textures," in *Proc. Int. Conf. Comput. Vis. Pattern Recognit.*, Jun. 2006, pp. 1932–1939.

[20] Y. Xu, H. Ji, and C. Fermüller, "Viewpoint invariant texture description using fractal analysis," *Int. J. Comput. Vis.*, vol. 83, no. 1, pp. 85–100, Jun. 2009.

[21] Z. Guo, Q. Li, J. You, D. Zhang, and W. Liu, "Local directional derivative pattern for rotation invariant texture classification," *Neural Comput. Appl.*, vol. 21, no. 8, pp. 1893–1904, Nov. 2012.

[22] Z. Guo, L. Zhang, and D. Zhang, "Rotation invariant texture classification using LBP variance (LBPV) with global matching," *Pattern Recognit.*, vol. 43, no. 3, pp. 706–719, Mar. 2010.

[23] Z. Guo, L. Zhang, and D. Zhang, "A completed modeling of local binary pattern operator for texture classification," *IEEE Trans. Image Process.*, vol. 19, no. 6, pp. 1657–1663, Jun. 2010.

[24] X. Tan and B. Triggs, "Enhanced local texture feature sets for face recognition under difficult lighting conditions," *IEEE Trans. Image Process.*, vol. 19, no. 6, pp. 1635–1650, Jun. 2010.

[25] P. Banerjee, A. K. Bhunia, A. Bhattacharyya, P. P. Roy, and S. Murala, "Local neighborhood intensity pattern—A new texture feature descriptor for image retrieval," *Expert Syst. Appl.*, vol. 113, pp. 100–115, Dec. 2018.

[26] S. K. Roy, B. Chanda, B. B. Chaudhuri, S. Banerjee, D. K. Ghosh, and S. R. Dubey, "Local directional ZigZag pattern: A rotation invariant descriptor for texture classification," *Pattern Recognit. Lett.*, vol. 108, pp. 23–30, Jun. 2018.

[27] T. P. Nguyen, N.-S. Vu, and A. Manzanera, "Statistical binary patterns for rotational invariant texture classification," *Neurocomputing*, vol. 173, pp. 1565–1577, Jan. 2016.

[28] G. Sucharitha and R. K. Senapati, "Biomedical image retrieval by using local directional edge binary patterns and Zernike moments," *Multimedia Tools Appl.*, vol. 79, pp. 1–18, Nov. 2019.

[29] T. Chakraborti, B. McCane, S. Mills, and U. Pal, "LOOP descriptor: Local optimal-oriented pattern," *IEEE Signal Process. Lett.*, vol. 25, no. 5, pp. 635–639, May 2018.

[30] A. Pillai, R. Soundrapandiyan, S. Satapathy, S. C. Satapathy, K.-H. Jung, and R. Krishnan, "Local diagonal extrema number pattern: A new feature descriptor for face recognition," *Future Gener. Comput. Syst.*, vol. 81, pp. 297–306, Apr. 2018.

[31] F. Ouslimani, A. Ouslimani, and Z. Ameur, "Rotation-invariant features based on directional coding for texture classification," *Neural Comput. Appl.*, vol. 31, no. 10, pp. 6393–6400, Oct. 2019.

[32] X. Wu and J. Sun, "Face recognition based on multi-scale local directional value," *Multimedia Tools and Applications*, vol. 79, pp. 1–17, Nov. 2019.

[33] T. Tuncer and S. Dogan, "Pyramid and multi kernel based local binary pattern for texture recognition," *J. Ambient Intell. Humanized Comput.*, vol. 11, pp. 1–12, May 2019.

[34] S. Chakraborty, S. K. Singh, and P. Chakraborty, "Cascaded asymmetric local pattern: A novel descriptor for unconstrained facial image recognition and retrieval," *Multimedia Tools Appl.*, vol. 78, pp. 1–20, May 2019.

[35] L. Armi and S. Fekri-Ershad, "Texture image Classification based on improved local Quinary patterns," *Multimedia Tools Appl.*, vol. 78, pp. 1–24, Feb. 2019.

[36] L. Kabbai, M. Abdellaoui, and A. Douik, "Image classification by combining local and global features," *Vis. Comput.*, vol. 35, no. 5, pp. 679–693, May 2019.

[37] J. Liu, Y. Chen, and S. Sun, "A novel local texture feature extraction method called multi-direction local binary pattern," *Multimedia Tools Appl.*, vol. 78, pp. 1–16, Feb. 2019.

[38] H.-C. Shih, H.-Y. Cheng, and J.-C. Fu, "Image classification using synchronized rotation local ternary pattern," *IEEE Sensors J.*, vol. 20, no. 3, pp. 1656–1663, Feb. 2020.

[39] D. Bhattacharjee and H. Roy, "Pattern of local gravitational force(PLGF): A novel local image descriptor," *IEEE Trans. Pattern Anal. Mach. Intell.*, early access, Aug. 1, 2019, doi: 10.1109/TPAMI.2019.2930192.

[40] I. El Khadiri, Y. El Merabet, Y. Ruichek, D. Chetverikov, and R. Touahni, "O3S-MTP: Oriented star sampling structure based multi-scale ternary pattern for texture classification," *Signal Process., Image Commun.*, vol. 84, May 2020, Art. no. 115830.

[41] T. Song, H. Li, F. Meng, Q. Wu, B. Luo, B. Zeng, and M. Gabbouj, "Noise-robust texture description using local contrast patterns via global measures," *IEEE Signal Process. Lett.*, vol. 21, no. 1, pp. 93–96, Jan. 2014.

[42] T. Song, H. Li, F. Meng, Q. Wu, and B. Luo, "Exploring space–frequency co-occurrences via local quantized patterns for texture representation," *Pattern Recognit.*, vol. 48, no. 8, pp. 2621–2632, Aug. 2015.

[43] A. Krizhevsky, I. Sutskever, and G. E. Hinton, "ImageNet classification with deep convolutional neural networks," in *Proc. Adv. Neural Inf. Process. Syst.*, 2012, pp. 1097–1105.

[44] K. Simonyan and A. Zisserman, "Very deep convolutional networks for large-scale image recognition," 2014, *arXiv:1409.1556*. [Online]. Available: http://arxiv.org/abs/1409.1556

[45] K. He, X. Zhang, S. Ren, and J. Sun, "Deep residual learning for image recognition," in *Proc. IEEE Conf. Comput. Vis. Pattern Recognit. (CVPR)*, Jun. 2016, pp. 770–778.

[46] L. Liu, S. Lao, P. W. Fieguth, Y. Guo, X. Wang, and M. Pietikainen, "Median robust extended local binary pattern for texture classification," *IEEE Trans. Image Process.*, vol. 25, no. 3, pp. 1368–1381, Mar. 2016.

[47] S. Chakraborty, S. K. Singh, and P. Chakraborty, "Local quadruple pattern: A novel descriptor for facial image recognition and retrieval," *Comput. Electr. Eng.*, vol. 62, pp. 92–104, Aug. 2017.

[48] M. Verma and B. Raman, "Local neighborhood difference pattern: A new feature descriptor for natural and texture image retrieval," *Multimedia Tools Appl.*, vol. 77, pp. 1–24, May 2017.

[49] Y. El Merabet and Y. Ruichek, "Local concave-and-convex micro-structure patterns for texture classification," *Pattern Recognit.*, vol. 76, pp. 303–322, Apr. 2018.

[50] L. Ji, Y. Ren, X. Pu, and G. Liu, "Median local ternary patterns optimized with rotation-invariant uniform-three mapping for noisy texture classification," *Pattern Recognit.*, vol. 79, pp. 387–401, Jul. 2018.

[51] S. Chakraborty, S. K. Singh, and P. Chakraborty, "Centre symmetric quadruple pattern: A novel descriptor for facial image recognition and retrieval," *Pattern Recognit. Lett.*, vol. 115, pp. 50–58, Nov. 2018.

[52] I. El Khadiri, M. Kas, Y. El Merabet, Y. Ruichek, and R. Touahni, "Repulsive-and-attractive local binary gradient contours: New and efficient feature descriptors for texture classification," *Inf. Sci.*, vol. 467, pp. 634–653, Oct. 2018.

[53] S. R. Dubey, S. K. Singh, and R. K. Singh, "Local wavelet pattern: A new feature descriptor for image retrieval in medical CT databases," *IEEE Trans. Image Process.*, vol. 24, no. 12, pp. 5892–5903, Dec. 2015.

[54] F. Tajeripour and S. Fekri-Ershad, "Developing a novel approach for stone porosity computing using modified local binary patterns and single scale retinex," *Arabian J. Sci. Eng.*, vol. 39, no. 2, pp. 875–889, Feb. 2014.

[55] S. Fekri-Ershad, "Bark texture classification using improved local ternary patterns and multilayer neural network," *Expert Syst. Appl.*, vol. 158, Nov. 2020, Art. no. 113509.

[56] M. Kas, Y. El Merabet, Y. Ruichek, and R. Messoussi, "Mixed neighborhood topology cross decoded patterns for image-based face recognition," *Expert Syst. Appl.*, vol. 114, pp. 119–142, Dec. 2018.

[57] I. El Khadiri, A. Chahi, Y. El Merabet, Y. Ruichek, and R. Touahni, "Local directional ternary pattern: A new texture descriptor for texture classification," *Comput. Vis. Image Understand.*, vol. 169, pp. 14–27, Apr. 2018.

[58] M. Hassaballah, H. A. Alshazly, and A. A. Ali, "Ear recognition using local binary patterns: A comparative experimental study," *Expert Syst. Appl.*, vol. 118, pp. 182–200, Mar. 2019.

[59] T. Tuncer, S. Dogan, and V. Ataman, "A novel and accurate chess pattern for automated texture classification," *Phys. A, Stat. Mech. Appl.*, vol. 536, Dec. 2019, Art. no. 122584.

[60] M. Kas, I. E. Khaidir, Y. E. Merabet, Y. Ruichek, and R. Messoussi, "Multi level directional cross binary patterns: New handcrafted descriptor for SVM-based texture classification," *Eng. Appl. Artif. Intell.*, vol. 94, Sep. 2020, Art. no. 103743.

[61] R. Lan, H. Lu, Y. Zhou, Z. Liu, and X. Luo, "An LBP encoding scheme jointly using quaternionic representation and angular information," in *Proc. Neural Comput. Appl.*, vol. 32, Jan. 2019, pp. 1–7.

[62] Q. Luo, X. Fang, Y. Sun, L. Liu, J. Ai, C. Yang, and O. Simpson, "Surface defect classification for hot-rolled steel strips by selectively dominant local binary patterns," *IEEE Access*, vol. 7, pp. 23488–23499, 2019.

[63] Y. El Merabet, Y. Ruichek, and A. El Idrissi, "Attractive-and-repulsive center-symmetric local binary patterns for texture classification," *Eng. Appl. Artif. Intell.*, vol. 78, pp. 158–172, Feb. 2019.

[64] T. Song, H. Li, F. Meng, Q. Wu, and J. Cai, "LETRIST: Locally encoded transform feature histogram for rotation-invariant texture classification," *IEEE Trans. Circuits Syst. Video Technol.*, vol. 28, no. 7, pp. 1565–1579, Jul. 2018.

[65] S. Chakraborty, S. K. Singh, and P. Chakraborty, "R-theta local neighborhood pattern for unconstrained facial image recognition and retrieval," *Multimedia Tools Appl.*, vol. 78, no. 11, pp. 14799–14822, Jun. 2019.

[66] H. Al-Marzouqi, Y. Hu, and G. AlRegib, "Texture retrieval using periodically extended and adaptive curvelets," *Signal Process., Image Commun.*, vol. 76, pp. 252–260, Aug. 2019.

[67] T. Song, J. Feng, L. Luo, C. Gao, and H. Li, "Robust texture description using local grouped order pattern and non-local binary pattern," *IEEE Trans. Circuits Syst. Video Technol.*, early access, Feb. 6, 2020, doi: 10.1109/TCSVT.2020.2972155.

[68] L. F. S. Scabini, L. C. Ribas, and O. M. Bruno, "Spatio-spectral networks for color-texture analysis," *Inf. Sci.*, vol. 515, pp. 64–79, Apr. 2020.

[69] A. Fernández, M. X. Álvarez, and F. Bianconi, "Image classification with binary gradient contours," *Opt. Lasers Eng.*, vol. 49, nos. 9–10, pp. 1177–1184, Sep. 2011.

[70] F. Bianconi, R. Bello-Cerezo, and P. Napoletano, "Improved opponent color local binary patterns: An effective local image descriptor for color texture classification," *J. Electron. Imag.*, vol. 27, no. 1, Dec. 2017, Art. no. 011002.

[71] M. Pietikainen and G. Zhao, "Two decades of local binary patterns: A survey," in *Proc. Adv. Independ. Compon. Anal. Learn. Mach.*, 2015, pp. 175–210.

ELMOKHTAR RACHDI (Member, IEEE) received the M.Sc. degree from Ibn Tofail University, Morocco, in 2006, where she is currently pursuing the Ph.D. degree in computer science. Her research interests include computer vision and information visualization.

YOUSSEF El MERABET received the M.Sc. degree from Ibn Tofail University, Morocco, in 2008, and the Ph.D. degree from the University of Technology of Belfort-Montbeliard, France, and Ibn Tofail University, in 2013. He is currently an Assistant Professor of computer science and technology with Ibn Tofail University. His research interests include computer vision and information visualization.

ZAHID AKHTAR (Senior Member, IEEE) received the Ph.D. degree in electronic and computer engineering from the University of Cagliari, Italy. He is currently an Assistant Professor with the Department of Network and Computer Security, State University of New York (SUNY) Polytechnic Institute, USA. Prior to that, he was a Research Assistant Professor with the University of Memphis, USA, and a Postdoctoral Fellow with the INRSEMT, University of Quebec, Canada, the University of Udine, Italy, Bahcesehir University, Turkey, and the University of Cagliari. His research interests include the computer vision and machine learning with applications to cybersecurity, biometrics, affect recognition, image and video processing, and audiovisual multimedia quality assessment.

ROCHDI MESSOUSSI received the Ph.D. degree in solid state physics from the University of Nantes, France, in 1990, and the master's degree in the use of technology for learning from the University of Strasbourg, in 2001. He is currently a Professor with Ibn Tofail University, Kénitra, Morocco, where he has been carrying out research about Human–Computer Interaction.

• • •